Hindawi Publishing Corporation
Advances in Materials Science and Engineering
Volume 2013, Article ID 578460, 8 pages
http://dx.doi.org/10.1155/2013/578460

Research Article

Hydrothermal Synthesis of Pt-, Fe-, and Zn-doped SnO_2 Nanospheres and Carbon Monoxide Sensing Properties

Weigen Chen,[1] Qu Zhou,[1] and Shudi Peng[2]

[1] *State Key Laboratory of Power Transmission Equipment & System Security and New Technology, Chongqing University, Chongqing 400030, China*
[2] *Chongqing Electric Power Research Institute, Chongqing 401123, China*

Correspondence should be addressed to Weigen Chen; weigench@cqu.edu.cn and Qu Zhou; zhouqu@cqu.edu.cn

Received 12 March 2013; Revised 23 July 2013; Accepted 24 July 2013

Academic Editor: Shivakiran Bhaktha

Pure and M-doped (M = Pt, Fe, and Zn) SnO_2 nanospheres were successfully synthesized via a simple and facile hydrothermal method and characterized by X-ray powder diffraction, field-emission scanning electron microscopy, and energy dispersive spectroscopy. Chemical gas sensors were fabricated based on the as-synthesized nanostructures, and carbon monoxide sensing properties were systematically measured. Compared to pure, Fe-, and Zn-doped SnO_2 nanospheres, the Pt-doped SnO_2 nanospheres sensor exhibits higher sensitivity, lower operating temperature, more rapid response and recovery, better stability, and excellent selectivity. In addition, a theoretical study based on the first principles calculation was conducted. All results demonstrate the potential of Pt dopant for improving the gas sensing properties of SnO_2-based sensors to carbon monoxide.

1. Introduction

Carbon monoxide (CO), mainly generated from the burning of fossil fuels and malfunctioning equipments, is a kind of colorless, tasteless, widespread, and toxic gas [1–5]. Simultaneously, CO is an important fault characteristic gas dissolved in power transformer oil and has been widely used in evaluating the insulation performance of running transformer [6–8]. Therefore, it is essential to develop high performance CO gas sensors for environmental monitoring and industrial applications [9–13].

Due to the advantages of simple fabrication process, low maintenance cost, and long useful life, metal oxide semiconductors, such as SnO_2 [14], ZnO [15], In_2O_3 [16], TiO_2 [17], WO_3 [18], and NiO [19], have been widely used for fabricating chemical gas sensors. Among these oxide sensors, SnO_2, as an interesting chemically and thermally stable n-type semiconductor with wide band gap energy and large exciton binding energy, is regarded as one of the most promising sensing materials against CO gas, and the development of SnO_2 sensors for CO detection has been the focus of numerous research works in the world [20–24]. However, there still exist some limitations needed to be further improved, such as low sensitivity, poor selectivity, and bad stability.

At present, numerous efforts have been made to improve the sensing properties of metal oxide semiconductor sensors, among which, the strategy of doping modification with various metallic elements, for example, noble metal [25, 26], rare-earth metal [27], transition metal [28], and metal oxide [29], has been proven effective. Due to unique catalytic and electronic activities, these dopants are highly commended for catalyzing various gas sensing reactions. The current reports on the sensing behaviors of various metals-doped SnO_2 are mainly based on trial-and-error experiments, and its gas sensing mechanism remains controversial. Till now, the first principles theoretical calculation has been successfully used to investigate structural [30], electronic [31], magnetism [32], optical [33], and gas sensing properties [34, 35] of semiconductor SnO_2.

To the best of our knowledge, reports on the synthesis of Pt, Fe and Zn-doped SnO_2 nanospheres and their sensing

properties against CO are rare, and there is no literature about an atomic level understanding of its sensing mechanism. For these reasons, an atomic level understanding of CO gas sensing behaviors of Pt-, Fe-, and Zn-doped SnO_2 is performed.

Herein, we present a simple, facile, and green hydrothermal synthesis of pure and M-doped (M = Pt-, Fe-, and Zn) SnO_2 nanospheres. To demonstrate the potential applications, chemical gas sensors were fabricated with the as-synthesized SnO_2 nanospheres, and CO gas sensing properties were investigated in detail. The Pt-doped SnO_2 nanospheres sensor exhibits significantly enhanced CO sensing performances in terms of high sensitivity, low operating temperature, better selectivity, rapid response and recovery time, and good reproducibility in comparison with those of pure, Fe-, and Zn-doped SnO_2 nanospheres. In addition, with the first principles, a theoretical calculation was performed to further understand its sensing mechanism.

2. Experimental

2.1. Synthesis and Characterization of SnO_2 Nanoparticles. Pt-, Fe-, and Zn-doped SnO_2 nanospheres were prepared by a simple and facile hydrothermal synthesis route [14]. All the raw chemicals are analytical-grade reagents purchased from Beijing Chemicals Co. Ltd. and used as received without any further purification.

The detailed synthesis process of Pt-doped SnO_2 nanospheres is as follows. Typically, 20 mL of absolute ethanol, 20 mL of distilled water, 5.0 mmol $SnCl_4 \cdot 5H_2O$, 0.10 mmol $H_2PtCl_6 \cdot 6H_2O$, and 30 mmol ammonia hydroxide were mixed together in a 100 mL capacity beaker and magnetically stirred at room temperature for 30 min. Then, the fully mixed precursor was transferred into a 100 mL Teflon-lined stainless steel autoclave, which was completely sealed and subsequently heated at 200°C for 24 h in an electric furnace to produce the precipitate. After cooling to room temperature, the prepared precipitate was harvested by centrifugation and washed with distilled water and absolute ethanol three times, respectively. Finally, the product was dried at 80°C in air for 24 h.

Fe- and Zn-doped SnO_2 nanospheres were obtained in the same process except that 0.10 mmol $FeCl_3 \cdot 6H_2O$ and $Zn(CH_3COO)_2 \cdot 2H_2O$ were added as the source of Fe^{3+} or Zn^{2+} ions, respectively. In this study, pure SnO_2 nanospheres were also synthesized via hydrothermal method for the purpose of comparison.

The crystalline structures of the as-prepared pure, Pt-, Fe-, and Zn-doped SnO_2 nanospheres were performed by X-ray powder diffraction (XRD) at room temperature using a Rigaku D/max-1200X diffractometer (Tokyo, Japan) with Cu $K_{\alpha 1}$ radiation (40 kV, 200 mA, and $\lambda = 1.5406$ Å). A Nova 400 Nano Field-emission scanning electron microscopy (FESEM, FEI, Hillsboro, OR, USA) equipped with an Oxford Inca 250 EDS energy-dispersive spectroscopy detector was used to characterize the surface morphologies and chemical compositions of the prepared samples.

2.2. Fabrication and Measurement of SnO_2-Based Sensors. Chemical gas sensors based on the as-synthesized SnO_2 nanospheres were fabricated as follows. First, the as-synthesized samples were mixed with diethanolamine and absolute ethanol at a weight ratio of 8 : 1 : 1 to form a paste. It was subsequently screen printed onto an alumina ceramic tube, where a pair of Au electrodes has been previously placed at each side. And then, the alumina ceramic tube was dried at 100°C for 2 h in air and sintered at 400°C for 2 h. Finally, an Ni-Cr heating wire was inserted into the tube to form a side-heated gas sensor. The structure diagram of the sensor is similar to that presented in our previous works [7, 14]. The as-prepared sensor was further aged at 200°C for a week in an aging test chamber to improve its stability and repeatability.

The gas sensing properties were measured by a CGS-8 intelligent gas sensing analysis system purchased from Beijing Elite Tech Co., Ltd., China. The operating temperature of the sensor could be adjusted precisely through varying the heating current of the Ni-Cr heater. When a smooth and stable baseline resistance was reached, a certain concentration of CO gas was injected into the test chamber. All tests were performed at constant environment temperature and relative humidity. Gas response in this study was defined as $S = R_a/R_g$, where R_a and R_g are the sensor resistance in air and in target gas, respectively [26]. The time taken by the sensor to achieve 90% of the total resistance change was designated as the response time in the case of gas adsorption or the recovery time in the case of gas desorption [4].

2.3. Computational Method. Based on the density functional theory (DFT), the first principles calculations were performed using the CASTEP code (Cambridge Sequential Total Energy Package) in this study [36–40]. Generalized gradient approximation (GGA) in the scheme of revised-Perdew-Burke-Ernzerhof (RPBE) was employed to describe the exchange and correlation functional between electrons. Interaction between nuclei and electrons was approximated with planewave ultrasoft pseudopotential [7, 34]. The valence electron configurations for C, O, and Sn atoms were chosen as $2s^2\ 2p^2$, $2s^2\ 2p^4$, and $5s^2\ 5p^2$, respectively, for structural and electronic calculations. The cut-off energy of the planewave was set at 380 eV throughout this work, which ensures a maximum root-mean-square convergent tolerance of 1.0×10^{-6} eV/atom. In the whole process of geometry optimization and energy calculation, atoms were freely allowed to relax in all directions.

3. Results and Discussion

3.1. Structural Characterization. X-ray powder diffraction measurement was firstly performed to check the crystalline structures of the synthesized nanostructures. Figure 1 shows the typical XRD patterns of the prepared pure, Pt-, Fe-, and Zn-doped SnO_2 samples. It can be clearly seen in Figure 1 that the synthesized samples are polycrystalline in nature and the XRD patterns of the prepared pure and M-doped SnO_2 powders are well corresponding with JCPDS card number 41-1445. All diffraction peaks can be perfectly indexed to the

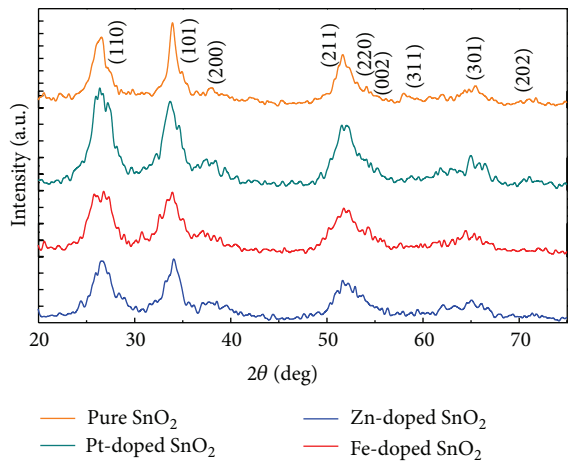

FIGURE 1: XRD patterns of pure, Pt-, Fe-, and Zn-doped SnO_2 nanospheres.

rutile SnO_2 phases, and due to the low amount of dopants (2 at%) in the samples, there is no indication of the presence of other metal oxide diffraction peaks, implying a high purity of our products.

An energy dispersive spectroscopy analysis was utilized to confirm the chemical compositions of the synthesized samples. Figure 2 shows the EDS spectra of pure and M-doped SnO_2 nanospheres. As shown in Figure 2(a), only Sn, O, C, and Cu peaks are observed for pure SnO_2, and no other peaks have been found. Nevertheless, characteristic peaks from Fe, Pt, and Zn elements are measured in Figures 2(b), 2(c), and 2(d), respectively. Simultaneously, the radius of Pt^{4+} (0.625 Å), Fe^{3+} (0.645 Å), and Zn^{2+} (0.72 Å) is obviously less than or nearly equal to that of Sn^{4+} (0.71 Å); so, it is believed Pt^{4+}, Fe^{3+}, and Zn^{2+} could be doped into the SnO_2 matrix. Thus, based on the EDS results, we believe that Pt^{4+}, Fe^{3+}, and Zn^{2+} ions have been successfully incorporated into the SnO_2 nanostructures [26].

Field-emission scanning electron microscopy was further used to research the surface structural characteristics of the prepared samples. Typical FESEM micrographs are recorded and shown in Figure 3. As seen in Figures 3(a)–3(d), beautiful nanospheres are observed for pure and M-doped SnO_2 nanostructures. These nanospheres are rather dispersed and highly uniform in shape and size. The diameters of the samples are ranging from 35 to 40 nm. On comparison of the morphology of pure SnO_2 with that of the M-doped samples, similar microstructure and surface morphology are observed, which indicates that the dopant of Pt^{2+}, Fe^{3+}, and Zn^{2+} ions affects the microstructure and morphology of SnO_2 nanostructures slightly.

3.2. Gas Sensing Properties. To investigate how the ions doped in SnO_2 nanospheres influence the gas sensing properties of the sensors, we first measured the gas responses of the pure and Pt-, Fe-, and Zn-doped sensors to 100 ppm of CO at a series of operating temperatures ranging from 100°C to 450°C. As shown in Figure 4 for each sensor, the gas response curve increases and arrives to its maximum at a certain temperature, namely, the optimum operating temperature, and then decreases rapidly with further increasing operating temperature. The optimum operating temperatures of the Pt-, Fe-, and Zn-doped SnO_2 sensors are measured to be about 300, 350, and 350°C, respectively. It is also observed that at a same working temperature, the Pt-doped SnO_2 sensor exhibits obviously higher gas response than that of pure, Fe-, and Zn-doped SnO_2 sensors. The highest gas response of the Pt-doped SnO_2 sensor is 33.12 at 300°C, while only 11.15, 13.42, and 16.89 for pure, Zn-, and Fe-doped sensors at 350°C.

Figure 5 represents the gas responses of the pure and Pt-, Fe-, and Zn-doped SnO_2 sensors as a function of CO gas concentration with sensor working at its own optimum operating temperature as measured above. As shown in Figure 5, each sensor exhibits a nearly linear gas response curve against CO with gas concentration in the range of 5–300 ppm. The Pt-doped SnO_2 sensor exhibits enhanced CO sensing response compared with pure, Fe-, and Zn-doped sensors, which implies Pt doping can effectively improve the gas response of SnO_2 sensor to CO gas. Thus, the SnO_2 nanosphere doped with Pt^{2+} is a promising CO sensing material for fabricating high response CO sensors.

It is well known that response and recovery characteristics are important for evaluating the performances of semiconductor oxide sensors. Figure 6 shows the response and recovery properties of the Pt-, Fe-, and Zn-doped SnO_2 nanospheres sensors to 100 ppm of CO gas at each optimum operating temperature. It can be seen in Figure 6 that compared with Fe- and Zn-doped SnO_2 nanospheres, the sensor based on 2 at% Pt-decorated SnO_2 nanospheres shows shortest response and recovery time (8 s and 12 s, resp.). Such a rapid response and recovery property could be attributed to the excellent electronic sensitization and catalytic activities of Pt ions.

The gas responses of the sensors to 200 ppm of CO gas were investigated in two months to investigate its stability and repeatability. The measurements were reported every 10 days. As shown in Figure 7, slight variation is observed for Pt-doped sensor during the long experimental cycle, while much higher fluctuations are performed for pure, Fe-, and Zn-doped sensors. All results demonstrate the Pt-doped sensor exhibits more prominent long-term stability and repeatability against CO than pure, Fe-, and Zn-doped SnO_2 nanospheres sensors.

Selectivity is another important characteristic for metal oxide semiconductor sensors, especially with potential interference gases. Figure 8 depicts the histogram of the gas responses of Pt-, Fe-, and Zn-doped SnO_2 sensors to 100 ppm of CO and potential interference gases, including CH_3OH, NH_3, H_2S, and NO. As shown in Figure 8, the sensor based on 2 at% Pt-doped SnO_2 nanospheres exhibits considerably lower response values to other potential interface gases at 300°C. All gas sensing properties measured above demonstrate the 2 at% Pt-doped SnO_2 nanospheres sensor particularly interesting for CO detection in practice. Based on the gas measurements above, we can conclude that Pt doping

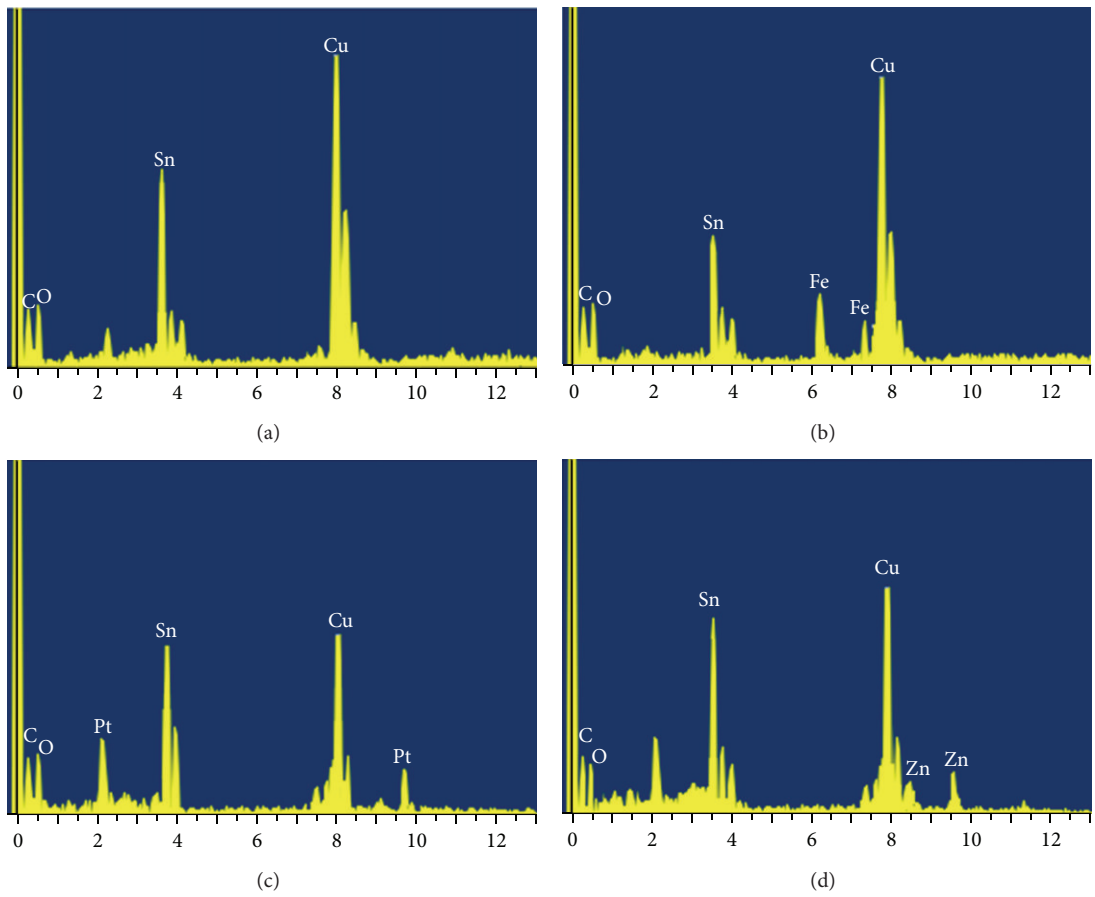

Figure 2: EDS spectra of pure, Fe-, Pt-, and Zn-doped SnO_2 nanospheres.

effectively enhances the gas sensing performances of SnO_2-based sensor to CO.

3.3. Theoretical Calculations. As a typical n-type semiconductor material, the gas sensing properties of SnO_2 are dominantly controlled by the surface. It is well known that the (110) surface is the most thermodynamically stable plane in tetragonal rutile SnO_2 [30, 31], and it has been widely used to investigate SnO_2 surface properties, such as structural, electronic, optical, magnetic, and gas sensing properties. Therefore, we performed a first principles calculation to go insight into how the doped metallic ions influence the gas sensing performances of SnO_2.

Figure 9(a) shows an established $2 \times 1 \times 1$ slab model of SnO_2 (110) surface, which is constituted of $Sn_{12}O_{24}$ with nine layers. To preserve symmetry, the top and bottom layers of the slab were taken to be identical. The central five layers were constrained at their bulk-like sites, and the surface and subsurface layers on either side of the slab were allowed to relax freely in all directions. A surface vacuum slab of 10 Å was added to avoid unnecessary interactions between the slabs, and then a $4 \times 2 \times 1$ supercell of $Sn_{48}O_{96}$ was employed.

One Sn atom was first substituted by Pt, Fe, or Zn atom in the surface or subsurface layers to obtain the doping model ($Sn_{47}MO_{96}$) with a doping ratio of 2.08%. Four probable doping configurations were illustrated as shown in Figure 9(b): substitution in Sn_{5C}, Sn_{6C}, sub-Sn_{5C} and sub-Sn_{6C}, cite, respectively. The doping formation energy E_f was defined as [34]

$$E_f = E\left(Sn_{47}MO_{96}\right) - E\left(Sn_{48}O_{96}\right) + \mu_{Sn} - \mu_M, \quad (1)$$

where $E\left(Sn_{47}MO_{96}\right)$ and $E\left(Sn_{48}O_{96}\right)$ represent the total energy of M-doped and pure SnO_2 supercells after geometry optimization, and μ_{Sn} and μ_M are the chemical potentials of each Sn and M atom in the bulk Sn and M crystal, respectively. According to the definition, the lower the doping formation energy E_f is, the more stability the doping model has.

As shown in Table 1, for each metal doping model, the doping formation energy of substitution in Sn_{5C} position is lower than that in Sn_{6C}, sub-Sn_{5C}, and sub-Sn_{6C} cites, respectively. Therefore, Pt, Fe, and Zn atoms are all prior to occupy the Sn_{5C} site on the top layer of SnO_2 (110) surface. In the following discussion, we mainly consider Pt, Fe, and Zn atoms substituted on Sn_{5C} site.

Figure 10 shows the calculated total density of states (DOS) of pure, Pt-, Fe-, and Zn-doped SnO_2 (110) surfaces. Compared with pure SnO_2, the DOS of M-doped SnO_2 (110) surface shifted downward, its band gap narrowed, and some new doping levels appeared near the Femi level, which could benefit charge transfer between SnO_2 valence band and

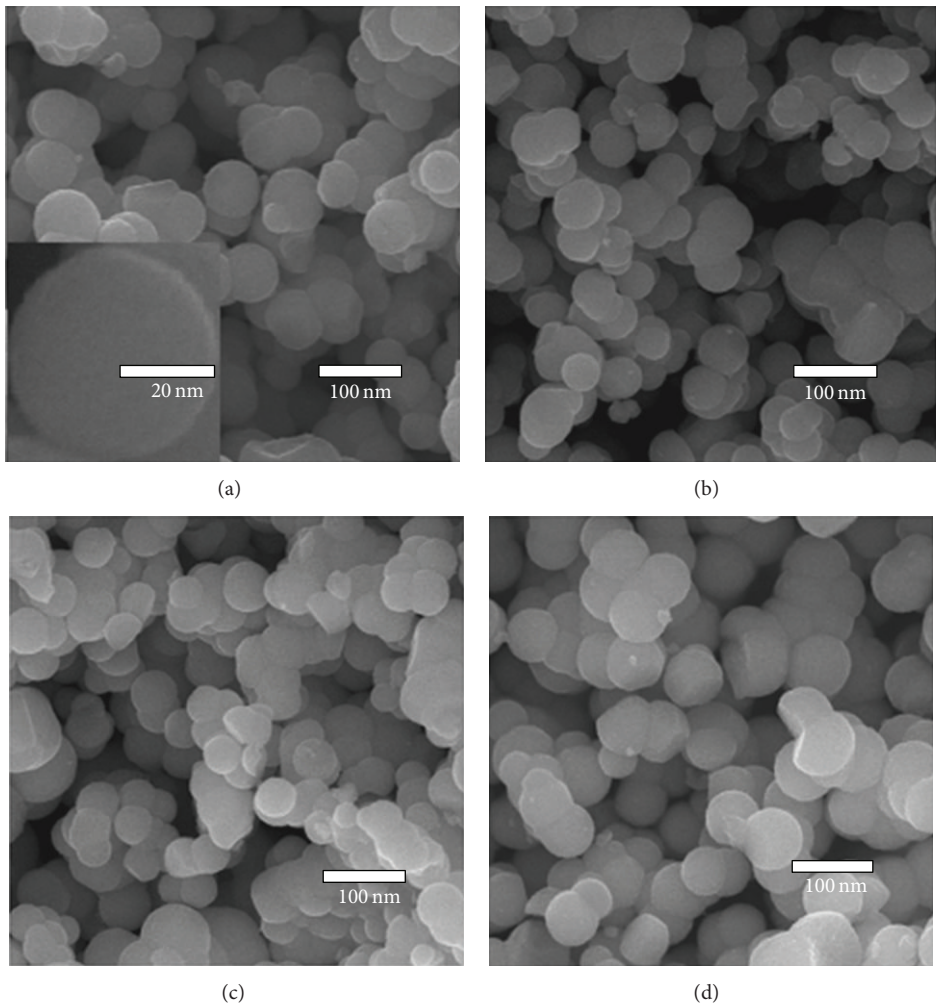

Figure 3: FESEM images of (a) pure, (b) Pt-, (c) Fe-, and (d) Zn-doped SnO_2 nanospheres.

Table 1: The doping formation energy of $Sn_{47}MO_{96}$.

Doping formation energy (eV)	Sn_{5C}	Sn_{6C}	Sub-Sn_{5C}	Sub-Sn_{6C}
E_f(Pt → Sn)	3.52	4.15	5.08	5.79
E_f(Fe → Sn)	3.79	4.37	5.13	6.08
E_f(Zn → Sn)	4.23	4.96	5.68	6.43

condition band and improve the gas sensing properties of the prepared SnO_2 based sensors.

As reported in former works, CO gas molecule prefers to be adsorbed on Sn_{5C} site with C end [7]; thus, in this study CO gas molecule was perpendicularly imported onto the Sn_{5C} atom with C end, and the initial vertical height between C atom of CO and Sn_{5C} atom of SnO_2 (110) surface was set as 2 Å, where C atom could bond with Sn_{5C} atom freely.

Figure 11 shows the partial density of states (PDOS) of CO gas molecule after adsorption. One can clearly see in Figure 11 that the PDOS of CO has a leftward moving trend and the moving range decreases in the order of Pt-, Fe-, Zn-doped and pure SnO_2 surfaces. As shown in (a), when CO was adsorbed on pure surface, almost no other changes were observed except a little of band shift. For Pt-doped one (b), the PDOS of CO assigned by 5σ orbits nearly vanishes totally, and the 4σ orbits also diminish mostly, which implies a strong chemical reaction and banding between C atom and Sn_{5C} atom. When CO was adsorbed on Fe-doped (c) and Zn-doped SnO_2 models, similar changes are observed but much slightly.

Further quantitative understanding can be obtained by analyzing the charge transfer between CO molecule and adsorption surface [34]. Based on the Mulliken population analysis, the corresponding change transfers are 0.06, 0.22, 0.10, and 0.08 e when CO molecule adsorbed on pure, Pt-, Fe-, and Zn-doped SnO_2 (110) surface. Electrons lost from CO are received by the SnO_2 surface, decreasing the height of barrier in the depletion region of SnO_2 and increasing the concentration of charge carriers. Thus, increasing output voltage and gas response were observed in the gas sensing analysis system.

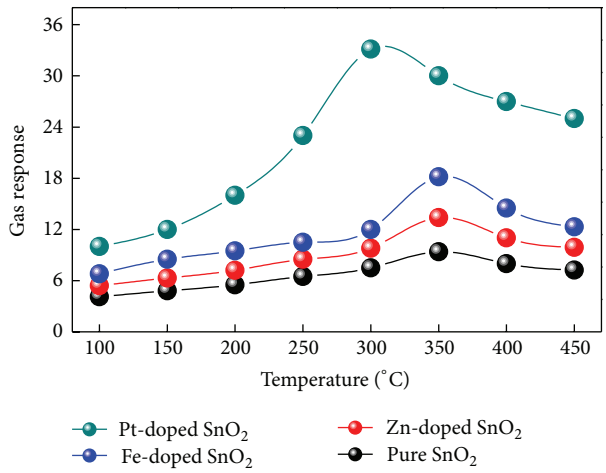

Figure 4: Gas responses of the sensors to 100 ppm of CO at various operating temperatures.

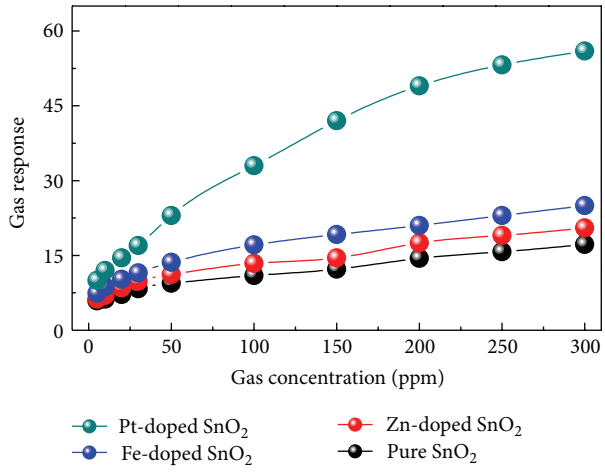

Figure 5: Gas responses of the sensors to different CO concentrations.

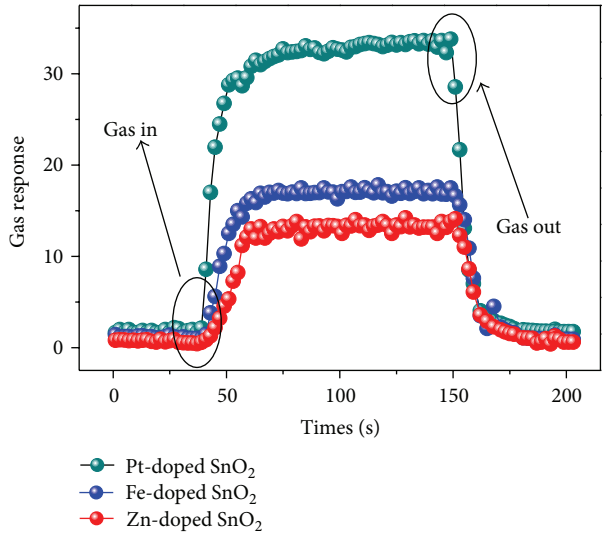

Figure 6: Response and recovery curves of the sensors to 100 ppm of CO.

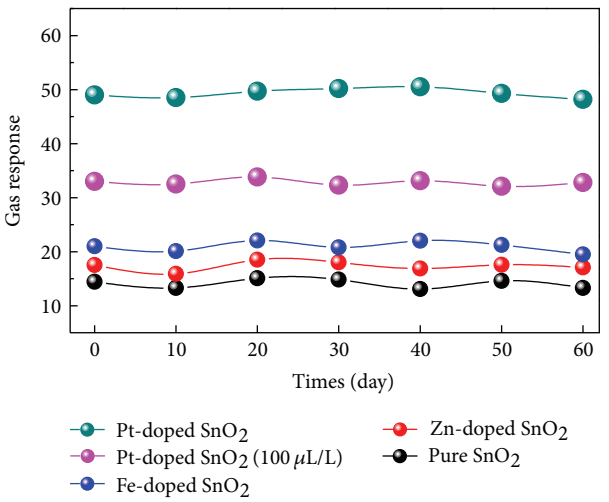

Figure 7: Stability and repeatability of the sensors to 100 ppm of CO.

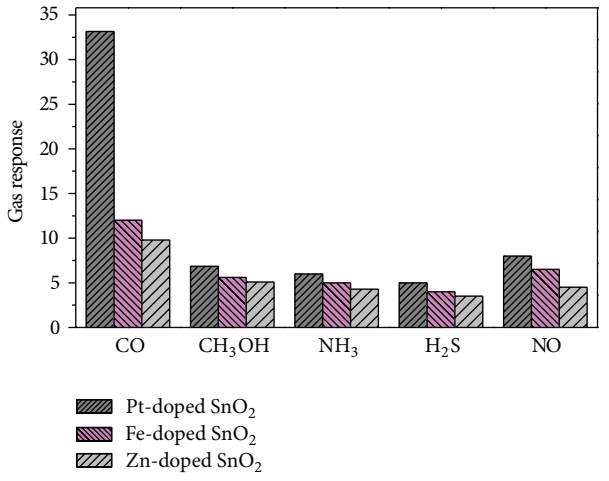

Figure 8: Selectivity of the 2 at% Pt-, Fe-, and Zn-doped SnO_2 sensors to 100 ppm of various gases at 300°C.

4. Conclusions

In conclusion, a simple hydrothermal synthesis of pure, 2 at% Pt-, Fe-, and Zn-doped SnO_2 nanospheres was demonstrated in the present paper. The as-synthesized nanostructures were characterized by XRD, EDS, and FESEM. Chemical gas sensors were fabricated, and CO gas sensing properties were discussed in detail. Comparative gas sensing tests show that the 2 at% Pt-doped SnO_2 nanospheres sensor exhibits excellent CO sensing performance in terms of low operating temperature, high response, rapid response and recovery time, and good reproducibility. Moreover, it shows good selectivity to potential interference gases. Based on the first principles calculation, its sensing mechanism was discussed. All results demonstrate that the Pt-doped SnO_2 nanospheres may be a potential candidate for fabricating high-performance CO gas sensors.

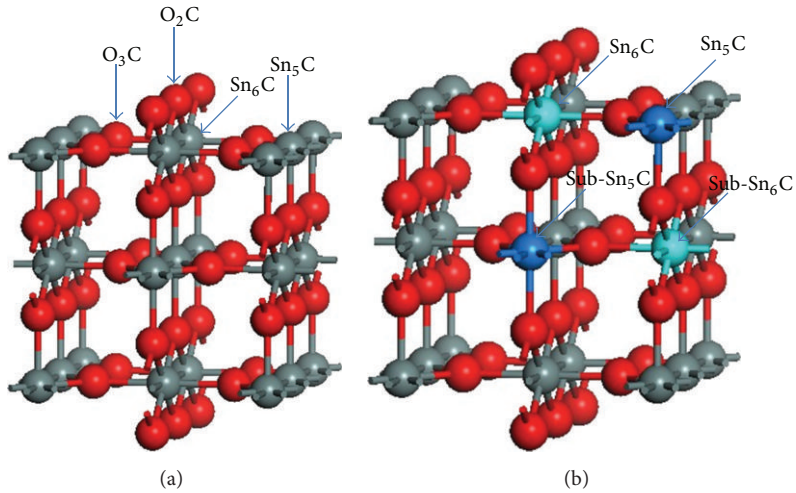

FIGURE 9: Schematic of (a) SnO_2 (110) surface model (b) doping and adsorption model.

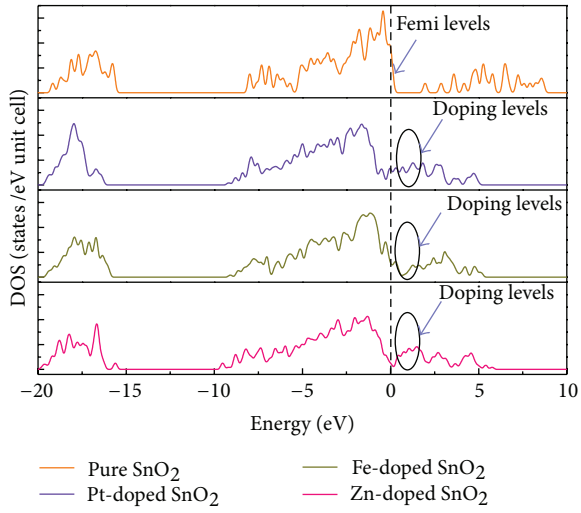

FIGURE 10: DOS of pure, Pt-, Fe-, and Zn-doped SnO_2 (110) surfaces.

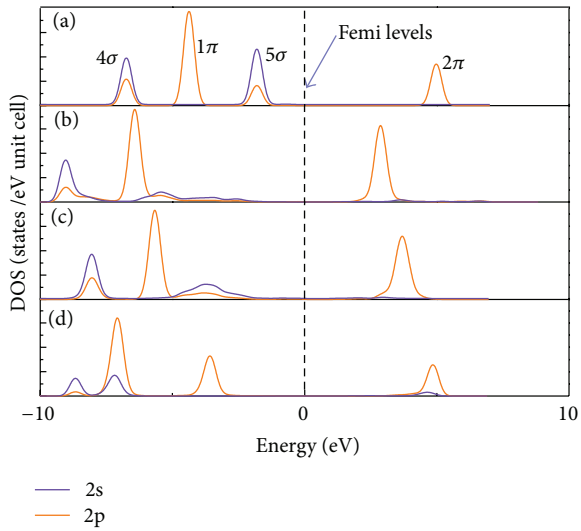

FIGURE 11: PDOS of CO molecule after adsorption.

Acknowledgments

This work was supported in part by the National Natural Science Foundation of China (nos. 51277185 and 51202302), National Special Fund for Major Research Instrumentation Development (no. 2012YQ160007), the Funds for Innovative Research Groups of China (no. 51021005), and China Postdoctoral Science Foundation (no. 2012M511904).

References

[1] G. F. Fine, L. M. Cavanagh, A. Afonja, and R. Binions, "Metal oxide semi-conductor gas sensors in environmental monitoring," *Sensors*, vol. 10, no. 6, pp. 5469–5502, 2010.

[2] A. Kolmakov, Y. X. Zhang, G. S. Cheng, and M. Moskovits, "Detection of CO and O_2 using tin oxide nanowire sensors," *Advanced Materials*, vol. 15, no. 12, pp. 997–1000, 2003.

[3] N. Bârsan and U. Weimar, "Understanding the fundamental principles of metal oxide based gas sensors; the example of CO sensing with SnO_2 sensors in the presence of humidity," *Journal of Physics Condensed Matter*, vol. 15, no. 20, pp. R813–R839, 2003.

[4] T. Zhang, L. Liu, Q. Qi, S. C. Li, and G. Y. Lu, "Development of microstructure In/Pd-doped SnO_2 sensor for low-level CO detection," *Sensors and Actuators B*, vol. 139, no. 2, pp. 287–291, 2009.

[5] L. L. Wang, H. M. Dou, Z. Lou, and T. Zhang, "Encapsuled nanoreactors (Au@ SnO_2): a new sensing material for chemical sensors," *Nanoscale*, vol. 5, no. 7, pp. 2686–2691, 2013.

[6] H. Teichert, T. Fernholz, and V. Ebert, "Simultaneous in situ measurement of CO, H_2O, and gas temperatures in a full-sized coal-fired power plant by near-infrared diode lasers," *Applied Optics*, vol. 42, no. 12, pp. 2043–2051, 2003.

[7] W. G. Chen, Q. Zhou, F. Wan, and T. Y. Gao, "Gas sensing properties and mechanism of nano-SnO_2-based sensor for

hydrogen and carbon monoxide," *Journal of Nanomaterials*, vol. 2012, Article ID 612420, 9 pages, 2012.

[8] Y. X. Yun, W. G. Chen, Y. Y. Wang, and C. Pan, "Photoacoustic detection of dissolved gases in transformer oil," *European Transactions on Electrical Power*, vol. 18, no. 6, pp. 562–576, 2008.

[9] K. J. Choi and H. W. Jang, "One-dimensional oxide nanostructures as gas-sensing materials: review and issues," *Sensors*, vol. 10, no. 4, pp. 4083–4099, 2010.

[10] Q. M. Konopacky, T. S. Barman, B. A. Macintosh, and C. Marois, "Detection of carbon monoxide and water absorption lines in an exoplanet atmosphere," *Science*, vol. 339, no. 6126, pp. 1398–1401, 2013.

[11] J. Yu, D. Zhao, X. L. Xu, X. Wang, and N. Zhang, "Study on RuO_2/SnO_2: novel and active catalysts for CO and CH_4 oxidation," *ChemCatChem*, vol. 4, no. 8, pp. 1122–1132, 2012.

[12] R. Q. Wu, M. Yang, Y. H. Lu, Y. P. Feng, Z. G. Huang, and Q. Y. Wu, "Silicon carbide nanotubes as potential gas sensors for CO and HCN detection," *Journal of Physical Chemistry C*, vol. 112, no. 41, pp. 15985–15988, 2008.

[13] R. X. Wang, D. J. Zhang, W. Q. Sun, Z. Han, and C. B. Liu, "A novel aluminum-doped carbon nanotubes sensor for carbon monoxide," *Journal of Molecular Structure: THEOCHEM*, vol. 806, no. 1–3, pp. 93–97, 2007.

[14] W. Zeng, B. Miao, Q. Zhou, and L. Y. Lin, "Hydrothermal synthesis and gas-sensing properties of variety low dimensional nanostructures of SnO_2," *Physica E*, vol. 47, no. 1, pp. 116–121, 2013.

[15] H. Gong, J. Q. Hu, J. H. Wang, C. H. Ong, and F. R. Zhu, "Nano-crystalline Cu-doped ZnO thin film gas sensor for CO," *Sensors and Actuators B*, vol. 115, no. 1, pp. 247–251, 2006.

[16] J. T. McCue and J. Y. Ying, "SnO_2-In_2O_3 nanocomposites as semiconductor gas sensors for CO and NO_x Detection," *Chemistry of Materials*, vol. 19, no. 5, pp. 1009–1015, 2007.

[17] Z. Y. Li, H. G. Zhang, W. Zheng et al., "Highly sensitive and stable humidity nanosensors based on LiCl doped TiO_2 electrospun nanofibers," *Journal of the American Chemical Society*, vol. 130, no. 15, pp. 5036–5037, 2008.

[18] X.-L. Li, T.-J. Lou, X.-M. Sun, and Y.-D. Li, "Highly sensitive WO_3 hollow-sphere gas sensors," *Inorganic Chemistry*, vol. 43, no. 17, pp. 5442–5449, 2004.

[19] L. L. Wang, Z. Lou, R. Wang, T. Fei, and T. Zhang, "Ring-like PdO-NiO with lamellar structure for gas sensor application," *Journal of Materials Chemistry*, vol. 22, no. 25, pp. 12453–12456, 2012.

[20] C. S. Moon, H.-R. Kim, G. Auchterlonie, J. Drennan, and J.-H. Lee, "Highly sensitive and fast responding CO sensor using SnO_2 nanosheets," *Sensors and Actuators B*, vol. 131, no. 2, pp. 556–564, 2008.

[21] L. H. Qian, K. Wang, Y. Li, H. T. Fang, Q. H. Lu, and X. L. Ma, "CO sensor based on Au-decorated SnO_2 nanobelt," *Materials Chemistry and Physics*, vol. 100, no. 1, pp. 82–84, 2006.

[22] R. M. Prasad, A. Gurlo, R. Riedel, M. Hübner, N. Barsan, and U. Weimar, "Microporous ceramic coated SnO_2 sensors for hydrogen and carbon monoxide sensing in harsh reducing conditions," *Sensors and Actuators B*, vol. 149, no. 1, pp. 105–109, 2010.

[23] A. Köck, A. Tischner, T. Maier et al., "Atmospheric pressure fabrication of SnO_2-nanowires for highly sensitive CO and CH_4 detection," *Sensors and Actuators B*, vol. 138, no. 1, pp. 160–167, 2009.

[24] U.-S. Choi, G. Sakai, K. Shimanoe, and N. Yamazoe, "Sensing properties of Au-loaded SnO_2-Co_3O_4 composites to CO and H_2," *Sensors and Actuators B*, vol. 107, no. 1, pp. 397–401, 2005.

[25] W. G. Chen, Q. Zhou, T. Y. Gao, X. P. Su, and F. Wan, "Pd-doped SnO_2-based sensor detecting characteristic fault hydrocarbon gases in transformer oil," *Journal of Nanomaterials*, vol. 2013, Article ID 127345, 9 pages, 2013.

[26] W. Zeng, T. M. Liu, D. J. Liu, and E. J. Han, "Hydrogen sensing and mechanism of M-doped SnO_2 (M = Cr^{3+}, Cu^{2+} and Pd^{2+}) nanocomposite," *Sensors and Actuators B*, vol. 160, no. 1, pp. 455–462, 2011.

[27] Q. Qi, T. Zhang, X. Zheng et al., "Electrical response of Sm_2O_3-doped SnO_2 to C_2H_2 and effect of humidity interference," *Sensors and Actuators B*, vol. 134, no. 1, pp. 36–42, 2008.

[28] L. Liu, C. C. Guo, S. C. Li, L. Y. Wang, Q. Y. Dong, and W. Li, "Improved H_2 sensing properties of Co-doped SnO_2 nanofibers," *Sensors and Actuators B*, vol. 150, no. 2, pp. 806–810, 2010.

[29] W. Zeng, T. M. Liu, and Z. C. Wang, "Enhanced gas sensing properties by SnO_2 nanosphere functionalized TiO_2 nanobelts," *Journal of Materials Chemistry*, vol. 22, no. 8, pp. 3544–3548, 2012.

[30] J. Oviedo and M. J. Gillan, "Energetics and structure of stoichiometric SnO_2 surfaces studied by first-principles calculations," *Surface Science*, vol. 463, no. 2, pp. 93–101, 2000.

[31] J. Oviedo and M. J. Gillan, "First-principles study of the interaction of oxygen with the SnO_2(1 1 0) surface," *Surface Science*, vol. 490, no. 3, pp. 221–236, 2001.

[32] C.-W. Zhang, P.-J. Wang, and F. Li, "First-principles study on surface magnetism in Co-doped (110) SnO_2 thin film," *Solid State Sciences*, vol. 13, no. 8, pp. 1608–1611, 2011.

[33] Y. Li, X. Zhao, and W. L. Fan, "Structural, electronic, and optical properties of Ag-doped ZnO nanowires: first principles study," *Journal of Physical Chemistry C*, vol. 115, no. 9, pp. 3552–3557, 2011.

[34] Z. Wen, L. Tian-Mo, and L. Xiao-Fei, "Hydrogen sensing properties of low-index surfaces of SnO_2 from first-principles," *Physica B*, vol. 405, no. 16, pp. 3458–3462, 2010.

[35] Y. B. Xue and Z. A. Tang, "Density functional study of the interaction of CO with undoped and Pd doped SnO_2(1 1 0) surface," *Sensors and Actuators B*, vol. 138, no. 1, pp. 108–112, 2009.

[36] S. Santucci, S. Picozzi, F. di Gregorio et al., "NO_2 and CO gas adsorption on carbon nanotubes: experiment and theory," *The Journal of Chemical Physics*, vol. 119, no. 20, pp. 10904–10910, 2003.

[37] W. An, X. J. Wu, and X. C. Zeng, "Adsorption of O_2, H_2, CO, NH_3, and NO_2 on ZnO nanotube: a density functional theory study," *The Journal of Physical Chemistry C*, vol. 112, no. 15, pp. 5747–5755, 2008.

[38] J. D. Prades, A. Cirera, J. R. Morante, J. M. Pruneda, and P. Ordejón, "Ab initio study of NOx compounds adsorption on SnO_2 surface," *Sensors and Actuators B*, vol. 126, no. 1, pp. 62–67, 2007.

[39] O. Leenaerts, B. Partoens, and F. M. Peeters, "Adsorption of H_2O, NH_3, CO, NO_2, and NO on graphene: a first-principles study," *Physical Review B*, vol. 77, no. 12, Article ID 125416, 6 pages, 2008.

[40] M. M. Islam, M. Calatayud, and G. Pacchioni, "Hydrogen adsorption and diffusion on the anatase TiO_2(101) surface: a first-principles investigation," *Journal of Physical Chemistry C*, vol. 115, no. 14, pp. 6809–6814, 2011.